CBPF-NF-049/03

Nuclear photofissility of ^{nat}Pb and ^{232}Th at energies above the pion photoproduction threshold*

O A P Tavares[1], S B Duarte[1], A Deppman[2] and V P Likhachev[2]

[1]Centro Brasileiro de Pesquisas Físicas-CBPF/MCT,
Rua Dr. Xavier Sigaud 150, 22290-180 Rio de Janeiro-RJ, Brazil

[2]Instituto de Física, Universidade de São Paulo, Caixa Postal 66318
05315-970 São Paulo-SP, Brazil

Abstract – A new, simple approach based on the intranuclear cascade plus the evaporation--fission competition mechanisms of photonuclear reactions has been developed to calculate fissility values at energies above ∼200 MeV. This approach has been successfully used in explaining fissility data for ^{nat}Pb and ^{232}Th target nuclei at energies up to 3.8 GeV recently obtained at the Thomas Jefferson Laboratory. Predictions of photofissility up to 5-6 GeV for these nuclei are also given.

Key-words: Photonuclear reactions; Photofission; Photofissility; Heavy target nuclei.

*Dedicated to Dr. J.D.T. Arruda-Neto on the occasion of his 60^{th} birthday.

1 Introduction

The interaction of intermediate-energy photons ($E_\gamma \gtrsim 200$ MeV) with complex nuclei has received much attention from researchers nowadays in view of, at least, four main reasons: i) the availability of high-quality monochromatic photon beams generated by the tagged photon technique, and, in particular, the development of high-performance parallel-plate avalanche detectors (PPAD) for fission fragments, thus allowing to obtain photofission cross section data with uncertainty not greater than ∼5% (actinide targets) or ∼12% (pre-actinide targets) [1- 10]; ii) the study of the behavior of the Δ resonance and other baryon resonances inside the nucleus to promote a better understanding of the photoabsorption mechanisms by the struck nucleus [11]; iii) the investigation of the so-called shadowing effect in photonuclear reactions which is apparent at higher incident photon energies (say, $E_\gamma \gtrsim 1.2$ GeV), resembling to a hadronic process of photonuclear interaction which has been described in the context of the Vector Dominance Model (VDM), but not yet completely understood [12,13]; and iv) the possibility of formation of rare, exotic nuclei (i.e., nuclei with unusual neutron-to-proton ratio) during the statistical de-excitation mechanism suffered by the compound nucleus resulting after the primary photoabsorption process in the target nucleus; the unusual properties of such exotic nuclei may influence the yield of the final spallation products, and this may become a question of current interest [14].

The simultaneous photofission cross section measurements carried out very recently at the Thomas Jefferson Laboratory on a number of actinide target nuclei and natural lead using tagged photons in the range ∼0.2-3.8 GeV and PPAD-detectors for detection of fission fragments [9,10] made it possible to extract important conclusions about the nuclear photoabsorption and fissility of these nuclei such as i) the ^{237}Np photofissility is very close to unity in the whole energy interval, thus indicating that its photofission cross section is almost completely equal to the total photoabsorption cross section; ii) the concept of a "Universal Behavior" for photoabsorption in complex nuclei, i.e. the independence on mass number of the total photoabsorption cross section per nucleon, is practically confirmed; iii) the photofissility for all other actinide nuclei (uranium isotopes and thorium) is less than unity, therefore their photofission cross section does not represent the photoabsorption cross section for these nuclei; iv) for all nuclei studied a shadowing effect is clearly manifested at photon energies greater than 1.3 GeV or so ; v) the $^{\rm nat}$Pb fissility relative to ^{237}Np increases from 2.5% at ∼0.2 GeV to about 7% at ∼0.6 GeV, and then it increases very slowly to a value of ∼7.5% near 4 GeV. About this latter point, it

should be mentioned that this is the first time photofissility data of excellent quality have been obtained for a non-actinide nucleus, covering a large energy region of photonuclear absorption, starting from near the pion photoproduction threshold and extending to ∼4 GeV where some expected shadowing effect is clearly seen.

Since photofissility data for actinide targets have been already analysed in some detail [10,15], we decided in the present work to focus attention on the newest photofissility data of ^{nat}Pb reported by Cetina *et al* [9,10]. Very recently, results of a more detailed and refined description of photofission reactions in actinide nuclei covering a large energy range (∼0.07−4.0 GeV) for the incident photon became available [16]. This so-called RELDIS Monte-Carlo code has shown to work quite well, but only qualitatively for ^{232}Th [16]. Therefore, the fissility data for ^{232}Th by Cetina *et al* [10] have also been included in the analysis of the present work. Here, photofissility data will be analysed in the framework of a phenomenological, semi-empirical way, aiming to obtain average calculated fissility values from an approach which has been developed for the first time in describing the intermediate-energy photofission reaction yields in the entire energy range of ∼0.2−3.8 GeV covered by the measured photofission cross section data. The current Monte Carlo calculations of photon-induced intranuclear cascade and fission-evaporation competition processes [4,13,15-23] are, in the present approach, replaced by a direct calculation of the total fission probability for the average excited residual nucleus formed after the rapid photoabsorption process in the target nucleus.

2 Semiempirical approach to photofission reactions

Following the generally accepted, current two-step model for intermediate-energy photofission reactions, the incoming photon interacts with one nucleon or a cluster of nucleons (quasi-deuteron) where pions, baryon resonances, and recoiling nucleons initiate a rapid ($\sim 10^{-23}$s) intra-nuclear cascade process during which energy is transferred to other nucleons, secondary pions and/or other recoiling nucleons may be generated inside the nucleus, some of these particles may escape from or be absorbed by the nucleus, and so on. At the end of the cascade process a residual, excited nucleus remains, and after thermodynamic equilibrium was reached, fission may occur as a result of a slow mechanism of competition between particle evaporation (neutron, proton, alpha particle, deuteron, tritium, and other) and fission experienced by the excited cascade residual.

Monte Carlo calculations are, at present, the main tool to describe quantitatively both the cascade and fission-evaporation competition processes, as well as to obtain

the total fission probabilities (photofissility values) for a number of photofission reaction cases. However, for cases where the target nucleus is expected to have low fissility-values (pre-actinide, intermediate-mass, and less massive nuclei), the available codes may reveal themselves very time-consuming in obtaining a calculated fissility-curve of acceptable uncertainty over a large energy-interval such as ∼0.2−4.0 GeV. This fact led us to develop an alternative method to evaluate nuclear photofissility-values when they are expected to be not greater than ∼50%, as it is the case for nuclei of $Z \leq 90$ and $A \leq 232$.

The target nucleus is considered to be a degenerate Fermi gas of non-interacting neutrons and protons confined within a spherically symmetric nuclear potential of radius R, the value of which is given by the equivalent root-mean-square radius of the nuclear charge distribution, i.e.

$$R = (5/3)^{1/2} < r^2 >^{1/2} , \tag{1}$$

where the value of $< r^2 >^{1/2}$ is taken from [23]. The Fermi energies for neutrons (E_f^n) and protons (E_f^p), as well as the respective cut-off energies, (E_c^n) and (E_c^p) , have been calculated by the usual way (the cut-off energy is defined as the Fermi energy plus the binding energy of the loosest nucleon plus, in the case of protons, the Coulomb energy at surface; binding energy values are those reported in [25]). By assuming $^{\rm nat}$Pb $\equiv$ ^{207}Pb, the values of the quantities mentioned above for $^{\rm nat}$Pb and ^{232}Th targets are practically the same for both nuclei, and they amount to $E_c^p \approx 51$ MeV and $E_c^n \approx 45$ MeV. The neutron and proton cut-off energies are the essential quantities to define the average post-cascade residual nuclei, as we shall see below.

2.1 Average post-cascade residual nucleus

An excited, residual nucleus is always produced at the end of the rapid intranuclear cascade process as a result of escaping (or not) of a small number of nucleons and/or pions. For an incident photon energy E_γ on a target nucleus (Z, A) two extreme situations can be envisaged: i) no proton, neutron, and/or pion are ejected at all during the cascade, i.e., $N_p^c = N_n^c = N_\pi^c = 0$, and, in this case, the maximum value of the excitation energy left to the cascade residual is given by

$$E^*_{max} \approx \begin{cases} E_\gamma, E_\gamma < B \\ B, E_\gamma \geq B, \end{cases} \tag{2}$$

where B is the total binding energy for (Z, A); ii) nearly all the incident energy E_γ is used to eject nucleons in the rapid cascade stage of the reaction and, in this case, the

maximum number of protons emitted is

$$N^c_{p_{max}} \approx \frac{Z}{A}\frac{E_\gamma}{E^p_c} \ , \tag{3}$$

and the maximum number of neutrons emitted is

$$N^c_{p_{max}} \approx \left(1 - \frac{Z}{A}\right) \ \frac{E_\gamma}{E^n_c} \ . \tag{4}$$

In this second extreme situation the minimum of excitation energy left to the produced residual nucleus is that energy with which an additional nucleon cannot be emitted during the cascade. The value for this energy is approximately given by the average value of the neutron and proton cut-off energies, i.e.,

$$E^*_{min} \approx \frac{1}{2}(E^n_c + E^p_c) \ . \tag{5}$$

Assuming that the average characteristics of the post-cascade residual nucleus ($\overline{Z}^*$, $\overline{A}^*$, $\overline{E}^*$) are defined by the simple mean between the extreme values of the quantities mentioned above, we can write

$$\overline{Z}^* \approx Z - \frac{E_\gamma}{2}\frac{Z}{A}\frac{1}{E^p_c} \ , \tag{6}$$

$$\overline{A}^* \approx A - \frac{E_\gamma}{2}\left[\frac{Z}{A}\frac{1}{E^p_c} + \left(1 - \frac{Z}{A}\right)\frac{1}{E^n_c}\right] \ , \tag{7}$$

$$\overline{E}^* \approx \begin{cases} \dfrac{E_\gamma}{2} + \dfrac{1}{4}(E^n_c + E^p_c), \ E_\gamma < B \\ \\ \dfrac{B}{2} + \dfrac{1}{4}(E^n_c + E^p_c), \ E_\gamma \geq B \ . \end{cases} \tag{8}$$

The above quantities represent the average atomic number (6), mass number (7), and excitation energy (8) of the post-cascade residual nuclei, and they are thought as the substitutes of their respective distribution functions in the sense that the average cascade residual is produced with probability equal to unity. Figure 1 summarizes the average properties of the photon-induced cascade process inside $^{\rm nat}$Pb target as a function of energy (Fig.1-a,b,c). The location of the produced residuals relative to the beta-stability line is also shown (Fig.1-d). It is interesting to compare results from the present, simple approach with those emerging from a detailed multicollisional Monte Carlo (MCMC)

calculation [26]. For 1-GeV incident photon on ^{207}Pb, equations (6-8) give $\overline{Z}^* = 78$, $\overline{A}^* = 196$, and $\overline{E}^* \approx 520$ MeV, while the MCMC code runned over 130 intranuclear cascade histories produces an average cascade residual as $\overline{Z}^* = 79\pm4$, $\overline{A}^* = 199\pm4$, and $\overline{E}^* = (400\pm60)$ MeV (spread of two standard deviations). These results show that the approximation introduced by the proposed assumptions (Eqs. (6-8)) can be considered satisfactory.

2.2 Total fission probability of post-cascade residuals

The second stage of the photofission reaction is described here by a fission-evaporation competition process starting from the average initial, excited residual nucleus ($\overline{Z}^*$, $\overline{A}^*$, $\overline{E}^*$) as represented schematically in Fig. 2. Neutron, proton, and alpha particle emissions are considered the modes of de-excitation which may compete more significantly with each other and with the fission mode for all subsequent residuals formed at each step along the evaporative sequence. The symbols in Fig. 2 represent the probability values of the different de-excitation channels, where the number in subscripts indicate the order of the different chance-fission or particle evaporation.

Fissionable evaporation residuals can be thought as being formed in generations. Let n be the order of a generation of residuals: $n = 1$ corresponds to the cascade residual, i.e., the first residual ($\overline{Z}^*$, $\overline{A}^*$, $\overline{E}^*$), and the partial fission probability is simply the first chance-fission probability

$$P_1^p = f_1. \tag{9}$$

For $n = 2$, formation of three evaporation residuals may occur, and the partial fission probability due to the chance-fission of the residuals in the second generation is

$$P_2^p = n_1 f_{2n} + p_1 f_{2p} + \alpha_1 f_{2\alpha} \ , \tag{10}$$

where n_1, p_1, and α_1 represent the probability for neutron, proton, and alpha particle emissions, respectively, and the f_2's are the second chance-fission probabilities. For $n = 3$, nine evaporation residuals may be formed, and the partial fission probability which results from the chance fission of the residuals in the third generation is

$$\begin{aligned} P_3^p = {} & n_1 n_2 f_{3,nn} + n_1 p_2 f_{3,np} + n_1 \alpha_2 f_{3,n\alpha} + \\ & p_1 n_2 f_{3,pn} + p_1 p_2 f_{3,pp} + p_1 \alpha_2 f_{3,p\alpha} + \\ & \alpha_1 n_2 f_{3,\alpha n} + \alpha_1 p_2 f_{3,\alpha p} + \alpha_1 \alpha_2 f_{3,\alpha\alpha} \ . \end{aligned} \tag{11}$$

Similar expressions can be written for the successive generations of residuals. Each term in (10) or (11) represents the chance-fission probability of the respective residual nucleus formed. The number of fissionable residuals which may be formed in the generation of order n is 3^{n-1}, and the total fission probability of the cascade residual is, therefore, given by

$$P_f^t(\overline{Z}^*, \overline{A}^*, \overline{E}^*) = \sum_{n=1}^{n_g} P_n^p \ . \tag{12}$$

The maximum number of generations of residuals is estimated as $n_g \approx \overline{E}^* / \overline{E}_{ev}$, where $\overline{E}_{ev}$ represents the average total energy removed from the system per particle evaporated (see below). The last fissionable residual in a generation is the one for which the excitation energy is still greater than its effective fission barrier height.

2.3 Probabilities of particle evaporation and fission

The routine calculation for the evaporation-fission competition process, i.e., the calculation of the probability-values for the neutron emission (n), proton emission (p), and alpha-particle emission (α) modes and the fission mode (f) has been already detailed in [13,21-23,27]. The method is based on the statistical model for particle evaporation from excited nuclei as proposed by Weisskopf [28] and the competition between neutron emission and fission as developed by Vandenbosch and Huizenga [29].

As input data we used for total nuclear binding energy, B, and neutron, proton, and alpha particle separation energies (S_n, S_p, and S_α, respectively) the values reported by Audi and Wapstra [25,30], while the ground-state fission barrier heights have been evaluated from data tabulated by Myers [31] following his droplet model of atomic nuclei.

For the level-density parameter of the residual nucleus after neutron evaporation, a_n, we adopted the expression

$$a_n = \tilde{a} \left\{ 1 + [1 - \exp(-0.051 E^*)] \ \frac{\Delta M}{E^*} \right\} \ \mathrm{MeV}^{-1} \tag{13}$$

proposed by Iljinov *et al* [32], in which ΔM is the shell correction in the calculated nuclear mass as tabulated in [31], and

$$\tilde{a} = 0.114A + 0.098A^{2/3} \ \mathrm{MeV}^{-1} \tag{14}$$

is the asymptotic value of a_n (a small correction on E^* due to pairing energy effects has been neglected in (13)) (for details see [32]).

Finally, the values for parameter $r = a_f/a_n$ (ratio of the level density parameter at the fission saddle point to a_n) have been obtained from a semiempirical determination of r-values which resulted from a systematic study of fissility on a number of experimental photofission cross section data measured in the quasi-deuteron energy region of photonuclear absorption on twelve target nuclei ranging from Sm to Bi [33]. Subsenquently, we have obtained r-values semiempirically for ^{232}Th from fissility data in the quasi-deuteron region of photonuclear absorption deduced from photofission cross section measurements by Sanabria *et al* [15] and Leprêtre *et al* [34]. An analysis of all such data allowed us to parametrize the r-values according to

$$r = 1 + \frac{\xi}{E^{*\eta}}, \tag{15}$$

where

$$\xi = \exp[0.150(222 - A)] \ , \qquad 150 \lesssim A \leq 210, \tag{16}$$

$$\xi = \exp[0.257(217 - A)] \ , \qquad 210 < A \leq 232, \tag{17}$$

$$\eta = 0.0352(235 - A) \ , \qquad 150 \lesssim A \leq 232, \tag{18}$$

which expressions are valid for excitation energies greater than ~ 40 MeV. In this way, it was possible to obtain a simple evaluation for the ratio r as function of both mass number and excitation energy like the quantity a_n (cf. Eq.(13)). The present parametrization of $r = a_f/a_n$ has proved to work quite well, even when applied to residuals located in the Po-Th region of nuclei where experimental information on level densities are not yet available at all.

2.4 Successive evaporation residuals

When a particle (neutron, proton, or alpha particle) was chosen to be evaporated from a certain residual i excited to an E_i^*-value, i.e., fission did not occur, a new evaporation residual, $i+1$, is formed with an excitation $E_{i+1}^* < E_i^*$. This process continues until the excitation energy available in the residual nucleus is not sufficient to allow the evaporation of another particle or fission to take place (the last, almost cold, residual formed in this way is known as spallation product, which finally de-excites by emission of gamma rays).

It is known that the kinetic energy of the emitted particles follows a Weisskopf distribution curve, and, therefore, the average total energy removed by the evaporation of one neutron, proton, or alpha particle from a certain residual can be calculated, respectively, as

$$\overline{E}_{ev_n} = S_n + 2\sqrt{\frac{E^* - S_n}{a_n}} \ , \tag{19}$$

$$\overline{E}_{ev_p} = (S_p + V_p) + 2\sqrt{\frac{E^* - (S_p + V_p)}{a_n}} \ , \tag{20}$$

$$\overline{E}_{ev_\alpha} = (S_\alpha + V_\alpha) + 2\sqrt{\frac{E^* - (S_\alpha + V_\alpha)}{a_n}} \tag{21}$$

where the approximation $a_n = a_p = a_\alpha$ is implicit.

In general, for the cascade residuals formed from the photointeraction with the Pb target the first-chance fission probability, f_1, is small ($\sim$0.3$-$1.6%) for at low photon energies (say, $E_\gamma \lesssim 300$ MeV, or $\overline{E}^* \lesssim 200$ MeV) the effective fission barriers ($B_f = B_{f_0}(1-\overline{E}^*/B)$) are relatively high ones, in such a way that evaporation of neutrons predominates. On the other hand, at higher incident photon energies the effective fission barriers become much lower in view of the nuclear temperature correction factor $(1 - \overline{E}^*/B) < 1$. However, in this case, the effective Coulomb barriers for the charged particles become also lower, therefore favoring the evaporation of these particles too. In addition, the fission probability for the successive residuals should become progressively lower because the excitation energy of the residuals along the evaporation chain decreases by $\sim$12$-$20 MeV per particle evaporated, therefore increasing the factor $(1-\overline{E}^*/B)$, at the same time that the effective fission barrier increases with decreasing of parameter Z^2/A. In the case of ^{232}Th target nucleus, the first-chance fission probability of average cascade residuals formed from the interaction of photons of energy $\sim$0.2$-$1.0 GeV amounts to $\sim$10$-$30%, for the effective fission barriers for these residuals are relatively low ones ($\sim$5$-$6 MeV) and comparable to neutron separation energies. At higher photon energies ($E_\gamma \geq 1$ GeV) the general behavior for the successive fissionable residuals is much the same as for those resulting from a $^{\rm nat}$Pb target . Therefore, the fission probability for successive evaporation residuals formed in a given generation n become lower and lower as compared to their precedent ones, i.e.,

$$f_{n_1} > f_{n_2} > f_{n_3} > \cdots \ . \tag{22}$$

2.5 Chance-fission probabilities

A chance-fission probability, q_{ni}, is a quantity defined by the product of the formation probability of residual i in the generation n times the fission probability of this residual, f_{ni} . To make this definition clear, we recall that each term in Eq.(11), for instance, represents the chance-fission probability of the residuals eventually formed in the third generation. In this example the partial fission probability is given by $P_3^p = \sum_{i=1}^{9} q_{3i}$. Certainly, a given evaporation residual may be formed through many different evaporation paths, and it may have different formation probabilities, thus leading to different chance-fission probabilities for this residual, but the number of residuals which may be formed in generation n is $N = 3^{n-1}$, and, therefore, the partial fission probability is

$$P_n^p = \sum_{i=1}^{N} q_{ni} \ . \tag{23}$$

We have used the routine calculation of the precedent sections to evaluate the chance-fission probabilities for the **most** and **least** probable evaporation paths starting from the initial, average cascade ^{196}Pt excited to 533 MeV, which is obtained from the interaction of 1.02-GeV photons with $^{\rm nat}$Pb target (Eqs.(6-8)). Figure 3 shows the q_{ni} values so obtained (points), where values for the second (3 points) and third (9 points) generations are made evident. Surprisingly, the q_{ni}-results lie (on a log-scale) very approximately on straight lines, one for the most likely evaporation path, i.e., for the greatest chance-fission probabilities in each generation of residuals, and another one for the least probable chance-fission of residuals eventually formed. This means that the chance-fission probability for any other evaporation residual formed in a given generation should be a value between these two linear limiting trends (Fig. 3). The most probable evaporation path can be considered as the main route of production of exotic nuclei via photonuclear interactions. In the example shown in Fig. 3 the nuclei produced from the average cascade residual ^{196}Pt come after successive evaporation of 4 neutrons, 1 alpha particle, 6 neutrons, 1 alpha particle, 4 neutrons, another alpha particle, 5 neutrons, and so on (^{182}Os, ^{174}W, ^{167}Hf can eventually be produced). These are on the region of proton-rich nuclei. On the opposite side, exotic nuclei with excess-neutrons may also be produced from successive charged particle emissions, such as ^{194}Os, ^{193}Re, and ^{192}W residuals in the example above.

Calculations have been also performed at other incident photon energies on $^{\rm nat}$Pb target, therefore producing different average cascade residuals as reported in Fig.4. We remark that the same pattern like the one exhibited in Fig. 3 is apparent in all cases

depicted in Fig. 4. Results for a ^{232}Th target are equally remarkable, as can be appreciated in Fig. 5. In all cases fluctuations of calculated points around the linear directions (Figs. 3,4, and 5) are mainly due to pairing plus shell effects.

The very interesting results reported above suggest parametrizing the chance-fission probabilities by an equation of the form

$$q_{ni} = f_1 e^{-(n-1)s_i} \ , \tag{24}$$

in which s_i denotes (on a ln-scale) the slope of the straight lines (Figs. 3,4, and 5). In what follows, we have organized the possible nuclides formed in each generation according to the order of decreasing of their chance-fission probabilities, i.e., $i = 1$ corresponds to the **most** probable evaporation sequence of residuals with chance-fission probabilities $q_{n1}(n > 1)$, and $s_1 = s_m$. The other extreme is $i = N = 3^{n-1}$, which corresponds to the **least** probable evaporation path of residuals eventually produced with chance-fission probabilities $q_{nN}(n > 1)$, and $s_N = s_l$ (see Fig. 3).

2.6 Partial fission probabilities and fissility

For a given generation of evaporation residuals (n fixed) the partial fission probability is the summation (23). We can obtain an estimation of the P_n^p's by taking simply the product of the number of residuals which may be formed in generation n times a certain average chance-fission probability, $\overline{q}_n$, i.e.,

$$P_n^p = \sum_{i=1}^{N} q_{ni} \approx \overline{q}_n \times 3^{n-1} \ . \tag{25}$$

The $\overline{q}_n$-values are, in turn, obtained from a certain average slope-value, $\bar{s}(s_m < \bar{s} < s_\ell)$, such that

$$\bar{q}_n = f_1 \mathrm{e}^{-(n-1)\bar{s}} \ . \tag{26}$$

Parameter $\bar{s}$ defines the slope of an average sequence of evaporation residuals which lie between the most and least probable sequences of residuals (dashed line in Fig. 3). In other words, the sum of the 3^{n-1} chance-fission probabilities as given by Eqs.(23,24) represents, for each generation of residuals, the chance-fission probability of an average, equivalent evaporation residual located on the $\bar{s}$-sequence.

The parameter $\bar{s}$ is introduced here to overcome the difficulty of calculating the $\sum_{n=1}^{n_g} 3^{n-1} \approx 3^{n_g}/2$ chance-fission probabilities which may appear during the de-excitation

process of the cascade residual (in a 2-GeV photointeraction with a $^{\rm nat}$Pb target, for instance, we would have to calculate $\sim 3 \times 10^{23}$ chance-fission probabilities!). One should remark that parameter $\bar{s}$ is, in a sense, model dependent, since one could take into account, for instance, not only neutron, proton, and alpha particle as the competitors with fission, but also deuteron, triton, ^{3}He, and other more complex clusters competing with fission. Besides, the input data for the basic nuclear quantities of the present approach, such as nuclear radius, ground-state fission barrier, level density parameters a_n and $r = a_f/a_n$, and others, certainly vary (if not substantially) with the source of information adopted. Therefore, the parameter $\bar{s}$ has to be considered an adjustable parameter, and thus its value has to be found semiempirically.

Finally, the average nuclear fissility is given by the total fission probability of the average cascade residual, and it is calculated as

$$\bar{f}_c(E_\gamma) = P_f^t(\bar{Z}^*, \bar{A}^*, \bar{E}^*) = \sum_n P_n^p = \bar{f}_1 \sum_n 3^{n-1} e^{-(n-1)\bar{s}} \tag{27}$$

which gives

$$\bar{f}_c = \frac{\bar{f}_1}{1 - 3e^{-\bar{s}}} \ . \tag{28}$$

In this way, for each incident photon energy on a target nucleus (i.e., an average cascade residual), fissility can be easily calculated provided the values of $\bar{f}_1$ and $\bar{s}$ are known. The average first-chance fission probability, $\bar{f}_1$, can be evaluated, for instance, from the three first-chance fission probabilities which define the most probable evaporation path (q_{11}, q_{21}, q_{31}) , and from those which define the least probable one(q_{11}, q_{23}, q_{39}) (see Figs. 4 and 5). By least-squares analysis one obtains

$$\bar{f}_1 = \left[\frac{q_{11}^5 \times q_{21} \times q_{23}}{(q_{31} \times q_{39})^{1/2}} \right]^{1/6} \ . \tag{29}$$

The values of $\bar{s}$ are, in turn, determined by taking the experimental fissility-values corresponding to the incident photon energy-values which produce average cascade residuals of both $\bar{Z}^*$ and $\bar{A}^*$ integer. The final values of $\bar{s}$ are then extracted from a smooth trend of $\bar{s}$ versus E_γ .

3 Results and Discussion

We have applied the present phenomenological, semiempirical, photofission approach of the preceding sections to analyse the photofissility experimental data for $^{\rm nat}$Pb and ^{232}Th

recently obtained at the Thomas Jefferson Laboratory by Cetina *et al* [10]. Results for $^{\rm nat}$Pb are summarized in Table 1 and Fig. 6. Both the relative and absolute photofissility data have been considered to define the average experimental photofissility-values, $\bar{f}_e = (f_r + f_a)/2$. The f_r-values are obtained directly from Table V of Ref. [10] by taking the ratio of the photofission cross section measurements listed in column 7 to those in column 2. These are showed as full circles in our Fig. 6. The absolute photofissility, f_a , is defined as the ratio of the photofission cross section to total photoabsorption cross section, and the f_a-values for $^{\rm nat}$Pb have been obtained here as the quotient of the entries listed in column 7 referred above to the corresponding (in energy) values from the smooth curve fitted to the existing photoabsorption cross section data for $^{\rm nat}$Pb (this curve is that one reported in Fig. 12-a of [10]). The f_a-values so obtained are represented as open circles in our Fig. 6. As one can see, the f_a-values are, in general, a few percent higher than thef_r-values at energies up to $\sim$1 GeV. This is because the independent total photoabsorption cross section measurements for Pb target do not include all the photoproduction channels other than the $(\gamma, x{\rm n}), x \gtrsim 2$, reaction. Above $\sim$1 GeV, however, both the f_r- and f_a-values are in quite complete agreement. Accordingly, the average experimental photofissilities for $^{\rm nat}$Pb (the $\bar{f}_e$-values) are listed in column 6 of our Table 1. Some of these data are interpolated values corresponding to E_γ-values previously chosen in such a way as to give both $\bar{Z}^*$ and $\bar{A}^*$ integer. Figure 6 also shows a few experimental points obtained at different laboratories in the quasi-deuteron region of photoabsorption [35-39]. A free, dashed line shows the trend of fissility in this low energy region.

The semiempirical $\bar{s}$-values which result when the average experimental photofissilities ($\bar{f}_e$) are used into Eq. (28) are represented by points (with error bars) plotted in the inset within Fig. 6. The smooth trend (full line) through these points gives the final values of parameter $\bar{s}$ (7th column in Table 1) to be used back in Eq. (28) in order to obtain the calculated photofissility-values (8th column in Table 1). Differences between $\bar{f}_e$ and $\bar{f}_c$ along the interval $\sim$0.2$-$4.0 GeV (last column of Table 1) are indeed small (less than $\sim$11%) if one considers the uncertainties of both $\bar{f}_e$ and $\bar{f}_c$. This means that the quantity $\bar{s}$ can be considered a good parameter for the present method of analysis of photofission reactions. In addition, the variation of $\bar{s}$ with E_γ (inset within Fig. 6) is not greater than $\sim$16%, showing a broad maximum in the range $\sim$0.3$-$1.0 GeV, and then it decreases slowly towards higher energies. A very similar trend for $\bar{s}$ (the dotted line in the inset graph) can be appreciated when the experimental photofissility of $^{\rm nat}$Pb relative to the ^{237}Np target (i.e., the f_r-values) is used into Eq. (28) instead of the $\bar{f}_e$-values. For the sake of comparison, the calculated, smooth fissility-curve is depicted in Fig. 6 as the

full line, where the shaded area indicates the error band associated with the $\bar{f}_c$-curve. The agreement between experimental (both f_r and f_a) and calculated fissility values can be considered very satisfactory. Calculated results of total fission probability for $^{\rm nat}$Pb following photoabsorption in the range $\sim$0.07$-$3.8 GeV obtained with the RELDIS Monte-Carlo code by Pshenichnov *et al* [16] are represented in Fig. 6 as the dotted line (variant B in their notation). Inspection on Fig. 6 shows that this calculated fissility-curve from Ref.[16] reveals a trend which does not differ greatly from the experimental one, but it is slightly underestimated at energies below 400 MeV, and overestimated above $\sim$1 GeV. The general behavior of $^{\rm nat}$Pb fissility with E_γ shows a monotonic increase of f from the lower energies up to $\sim$600 MeV, and then a tendency to saturate around 7.5% at energies up to at least $\sim$4 GeV. Besides, this saturation seems to be valid towards higher energies as indicated by the predictions of fissility carried out up to 6 GeV with the present approach (dash-dotted line in Fig. 6; see also Table 1).

Results for ^{232}Th target are given in Table 2 and Fig. 7. Here, the experimental fissility-values are obtained from data in Table V of Ref.[10] by taking the ratio of the photofission cross section measurements listed in column 6 to those in column 2. These are showed as full circles in our Fig. 7, and some of them are reported in column 6 of the present Table 2. As in the case for $^{\rm nat}$Pb target, some fissility data represent interpolated values corresponding to E_γ-values chosen to give both $\bar{Z}^*$ and $\bar{A}^*$ integer as listed in Table 2 [cf. Eqs.(6,7)]. Figure 7 also shows the twenty eight experimental fissility values (relative to ^{237}Np) measured from 68 to 264 MeV at the Saskatchewan Accelerator Laboratory (SAL) by Sanabria *et al* [15] (open circles). As regards the calculated curves, the same notation used in Fig. 6 is adopted here in the case for ^{232}Th target (fig. 7). Besides, all the analysis developed for $^{\rm nat}$Pb has been applied to ^{232}Th case to obtain the semiempirical values for parameter $\bar{s}$ (inset graph within Fig. 7), the calculated fissilities and their uncertainties (full line and shaded area in Fig. 7), and the respective deviations from the experimental data (last column in Table 2). Again, agreement between experimental and calculated fissilities as obtained by the present approach can be considered satisfactory. For comparison, calculated fissility-values with the RELDIS Monte-Carlo code (variant B in the notation in Ref.[16]) have been depicted in Fig. 7 (dotted curve), and they are seen $\sim$20$-$40% greater than the experimental values. It is not easy to explain the origin of this modest difference. Probably, the slightly enhanced (1.5$-$5.5%) values for the ratio $r = a_f/a_n$ adopted in Ref.[16] as compared to those calculated in Ref.[40] may be one of the main reasons for the mentioned difference.

Parameter $\bar{s}$ allows one to extract some information about the "point of fission" , i.e.

the location on the evaporation-fission competition sequence where fission takes place. Inspection of Eq.(27) shows that fissility is reached with the cumulative, partial fission probability which increases with the order of generation of residuals, n, but at a rate dictated by the $\bar{s}$-value. For example, in the case of 470 MeV photons interacting with a ^{nat}Pb target ($\sim$260 MeV of average excitation for the cascade residual) $\overline{s}$ equals to 1.33 (see Table 1), and a simple calculation indicates that only 6 or 7 generations of residuals are needed to reach, for instance, $\sim$80% of fissility. Since in this example it is possible to have nearly 22 generations of residuals, this means that fission is more likely to occur in the first third of the evaporative sequence. At higher energies, however, $\bar{s}$ may amount to only 1.15, and in these cases a higher number of generations of residuals is needed to obtain almost the total fission probability ($\sim$25 generations for 3.8 GeV photons), at the same time that more generations become possible of being formed ($\sim$50 in the case of 3.8-GeV photons), therefore making the "point of fission" uncertain to some extent. In other words, more energy available, more fission chances opened, therefore the point-of-fission becomes less defined (note that Eq.(28) imposes the limiting condition of $\bar{s} > \ln 3$).

4 Summary and Conclusion

Aiming to analyse the recent photofissility data of ^{nat}Pb and ^{232}Th target nuclei measured in the range $\sim$0.2$-$3.8 GeV at the Thomas Jefferson Laboratory we developed a new, simple approach to calculate the nuclear photofissilities semiempirically. This approach is based on the current, two-step model for intermediate-energy photonuclear reactions, i.e. a photon-induced intranuclear cascade followed by a fission-evaporation competition process for the excited, post-cascade nucleus. The distributions of atomic number, mass number, and excitation energy of the cascade residuals which would result from Monte Carlo calculations are replaced here by their respective average values ($\bar{Z}^*, \bar{A}^*, \bar{E}^*$). These have been defined as functions of the incident photon energy by means of simple expressions (Eqs. (6-8)) in which the neutron and proton cut-off energies play a fundamental role.

Next, the de-excitation of the average cascade residuals has been described by the usual way, where neutron, proton, and alpha particle emissions and fission are considered as the main de-excitation channels. In calculating the fission and particle emission probabilities of the different residuals, the particle separation energies, total nuclear binding energy, ground-state fission barrier heights, level density parameters, and nuclear radii have been taken from the current tables [25,30,31] or updated systematics [24,32,33].

A direct calculation of the total fission probability for the cascade residual (i.e., the target nucleus fissility) has been performed by taking into account all intermediate chance-fission probabilities of residuals eventually formed throughout the evaporation chain. This calculation has been simplified in view of the remarkable pattern exhibited by the chance-fission probability values, according to which the chances for fission are shown to lie between two rather linear (on log-scale) trends, one for the most probable, and another one for the least probable sequences of fissionable residuals (Figs. 3,4, and 5).

Finally, an adjustable parameter, $\bar{s}$, has been introduced, and its value (found semiempirically) defines an evaporative sequence in which the average, equivalent chance-fission probabilities of residuals belonging to the same generation are located. In this way, fissility-values can be easily calculated provided the first-chance fission probability ($\bar{f}_1$) and the $\bar{s}$-values are known (Eq. (28)). The experimental fissility data for both $^{\rm nat}$Pb and ^{232}Th nuclei have been described by the present scheme very satisfactorily (Figs. 6 and 7), at the same time that parameter $\bar{s}$ exhibits a rather monotonic trend in the entire photon energy range investigated here (insets within Figs. 6 and 7).

The present, semiempirical approach for photofission reactions can, surely, be refined by introducing, for instance, other de-excitation channels (deuteron, triton, lithium isotopes emission, etc) to compete with the fission channel. The present approach, as described in the previous sections, can certainly be applied to other photofission reaction cases, such as those for heavy actinide , pre-actinide, and intermediate-mass target nuclei (in the case of actinides it is necessary first to search for an appropriate expression for the ratio $r = a_f/a_n$ (Eq.15)). An upper limiting value for the incident photon energy, however, there exists (about 9 GeV in the case of heavy target nuclei), therefore the basic, simplified assumptions made to define the average characteristics of the post-cascade nucleus (section 2.1) should be reformulated to attain the very-high photon energy region. These will be the subject of work in the near future.

Acknowledgment - It is a pleasure to acknowledge the patient and qualified preparing of the drawings by M.G. Gonçalves. Partial support by the FAPESP Agency is also gratefully acknowledged.

References

[1] A.A. Kazakov, G.Ya. Kezerashvili, L.E. Lazareva, V.G. Nedorezov, A.N. Skrinsky, A.S. Sudov, G.M. Tumaikin, and Yu.M. Shatunov, Pis'ma Zh. Eksp. Teor. Fiz. **40**, 445 (1984) [JETP Letters **40**, 1271(1984)].

[2] J.Ahrens, J. Arends, P. Bourgeois, P. Carlos, J.L. Fallou, N. Floss, P. Garganne, S. Huthmacher, U. Kneissl, G. Mank, B. Mecking, H. Ries, R. Stenz, and A. Veyssière, Phys. Letters **146B**, 303 (1984).

[3] E.A. Arakelyan, A.R. Bagdsaryan, G.L. Bayatyan, G.S. Vartanyan, A.R. Voskanyan, N.K. Grigoryan, S.G. Knyazyan, A.T. Margaryan, G.G. Marikyan, and A.K. Papyan, Yad. Fiz. **52**, 1387 (1990) [Sov. J. Nucl. Phys. **52**, 878 (1990)].

[4] A.S. Iljinov, D.I. Ivanov, M.V. Mebel, V.G. Nedorezov, A.S. Sudov, and G.Ya. Kezerashvili, Nucl. Phys. **A539**, 263 (1992).

[5] N.Bianchi, A. Deppman, E. De Sanctis, A. Fantoni, P. Levi Sandri, V. Lucherini, V. Muccifora, E. Polli, A.R. Reolon, P. Rossi, M. Anghinolfi, P. Corvisiero, G. Gervino, L. Mazzaschi, V. Mokeev, G. Ricco, M. Ripani, M. Sanzone, M. Taiuti, A. Zucchiatti, R. Bergère, P. Carlos, P. Garganne, and A. Leprêtre, Phys. Letters **B299**, 219 (1993).

[6] N. Bianchi, A. Deppman, E. De Sanctis, A. Fantoni, P. Levi Sandri, V. Lucherini, V. Muccifora, E. Polli, A.R. Reolon, P. Rossi, A.S. Iljinov, M.V. Mebel, J.D.T. Arruda-Neto, M. Anghinolfi, P. Corvisiero, G. Gervino, L. Mazzaschi, V. Mokeev, G. Ricco, M. Ripani, M. Sanzone, M. Taiuti, A. Zucchiatti, R. Bergère, P. Carlos, P. Garganne, and A. Leprêtre, Phys. Rev. C **48**, 1785 (1993).

[7] Th. Frommhold, F. Steiper, W. Henkel, U. Kneissl, J. Ahrens, R. Beck, J. Peise, M. Schmitz, I. Anthony, J.D. Kellie, S.J. Hall, and G.J. Miller, Z. Phys. A **350**, 249 (1994).

[8] M.L. Terranova, G.Ya Kezerashvili, V. A. Kiselev, A. M. Milov, S.I. Mishnev, I. Ya. Protopopov, V.N. Rotaev, D.N. Shatilov, and O.A.P. Tavares, J. Phys. G: Nucl. Part. Phys. **22**, 1661 (1996).

[9] C. Cetina, B.L. Berman, W.J. Briscoe, P.L. Cole, G. Feldman, P. Heimberg, L.Y. Murphy, S. A. Philips, J.C. Sanabria, Hall Crannell, A. Longhi, D.I. Sober, and G.Ya. Kezerashvili, Phys. Rev. Letter **84**, 5740 (2000).

[10] C. Cetina, P. Heimberg, B.L. Berman, W.J. Briscoe, G. Feldman, L.Y. Murphy, Hall Crannell, A. Longhi, D.I. Sober, J.C. Sanabria, and G. Ya Kezerashvili, Phys. Rev. C **65**, 044622 (2002).

[11] N. Bianchi, V. Muccifora, E. De Sanctis, A. Fantoni, P Levi Sandri, E. Polli, A.R. Reolon, P. Rossi, M. Anghinolfi, P. Corvisiero, M. Ripani, M. Sanzone, M. Taiuti, and A. Zucchiatti, Phys. Rev. C **54**, 1688 (1996).

[12] N. Bianchi, E. De Sanctis, M. Mirazita, and V. Muccifora, Phys. Rev. C **60**, 064617 (1999).

[13] A. Deppman, O.A.P Tavares, S.B. Duarte, J.D.T. Arruda-Neto, M. Gonçalves, V.P. Likhachev, and E.C. de Oliveira, Phys. Rev. C **66**, 067601 (2002).

[14] D.R. Chakrabarty, S. K. Rathi, V.M. Datar, Suresh Kumar, E.T. Mirgule, A. Mitra, H.H. Oza, Nucl. Phys A **712**, 23 (2002).

[15] J.C. Sanabria, B.L. Berman, C. Cetina, P.L. Cole, G. Feldman, N.R. Kolb, R.E. Pywell, J.M. Vogt, V.G. Nedorezov, A.S. Sudov, and G.Ya Kezerashvili, Phys. Rev. C **61**, 034604 (2000).

[16] I.A. Pshenichnov, B.L. Berman, W.J. Briscoe, C. Cetina, G. Feldman, P. Heimberg, A.S. Iljinov, and I.I. Strakovsky, The George Washington University, Center for Nuclear Studies, Report arXiv: nucl-th/0303070v1, March 2003.

[17] B. Schröder, G. Andersson, and B. Forkman, Proceedings of the International Conference on Nuclear Physics (vol.1), Munich 27 Aug - 1 Sept, 1973 (North-Holland, 1973) p. 581.

[18] V. S. Barashenkov, F.G. Gereghi, A.S. Iljinov, G.G. Jonsson, and V.D. Toneev, Nucl. Phys. **A231**, 462 (1974).

[19] A.S. Iljinov, E.A. Cherepanov, and S.E. Chigrinov, Yad. Fiz. **32**, 322 (1980) [Sov. J. Nucl. Phys. **32**, 166 (1980)].

[20] A.S. Iljinov, M.V. Mebel, C. Guaraldo, V. Lucherini, E. De Sanctis, N. Bianchi, P. Levi Sandri, V. Muccifora, E. Polli, A.R. Reolon, P. Rossi, and S. Lo Ligro, Phys. Rev. C **39**, 1420 (1989).

[21] A.Deppman, O.A.P. Tavares, S.B. Duarte, E.C. de Oliveira, J.D.T. Arruda-Neto, S.R. de Pina, V.P. Likhachev, O. Rodríguez, J. Mesa, and M. Gonçalves, Phys. Rev. Letters **87**, 182701 (2001).

[22] A. Deppman, O.A.P. Tavares, S.B. Duarte, E.C. de Oliveira, J.D.T. Arruda-Neto, S.R. de Pina, V.P. Likhachev, O. Rodríguez, J. Mesa, and M. Gonçalves, Comp. Phys. Commun. **145**, 385 (2002).

[23]] A. Deppman, O.A.P. Tavares, S.B. Duarte, J.D.T. Arruda-Neto, M. Gonçalves, V.P. Likhachev, J. Mesa, E.C. de Oliveira, S.R. de Pina, and O. Rodríguez, Nucl. Instrum. Meth. Phys. Res. B, in press (2003).

[24] I. Angeli, International Nuclear Data Committee- INDC (HUN)-033, IAEA-NDS (September, 1999).

[25] G. Audi and A.H. Wapstra, Nucl. Phys **A565**, 66 (1993).

[26] M. Gonçalves, S. de Pina, D.A. de Lima, W. Milomen, E.L. Medeiros, and S.B. Duarte , Phys. Letters **B406**, 1 (1997).

[27] O.A.P. Tavares and M.L. Terranova, Z. Phys. A **343**, 407 (1992).

[28] V.F. Weisskopf, Phys. Rev. **52**, 295 (1937).

[29] R. Vandenbosch and J.R. Huizenga, in: *Nuclear Fission* (1st edition, pp 227, New York: Academic Press, 1973).

[30] G. Audi and A.H. Wapstra, Nucl. Phys. **A565**, 1 (1993).

[31]] W.D. Myers, in: *Droplet Model of Atomic Nuclei* (1^{st} Edition, pp.35, New York: Plenum Press, 1977).

[32]] A.S. Iljinov, M.V. Mebel, N. Bianchi, E. De Sanctis, C. Guaraldo, V. Lucherini, V. Muccifora, E. Polli, A.R. Reolon, and P. Rossi, Nucl. Phys. **A543**, 517 (1992).

[33] E. de Paiva, O.A.P. Tavares, and M.L. Terranova, J. Phys. G: Nucl. Part. Phys. **27**, 1435 (2001).

[34] A. Leprêtre, R. Bergère, P. Bourgeois, P. Carlos, J. Fajot, J.L. Fallou, P. Garganne, A. Veyssière, H. Ries, R. Göbel, U. Kneissl, G. Mank, H. Ströher, W. Wilke, D. Ryckbosch, and J. Jury, Nucl. Phys. A472, 533(1987).

[35] Yu. N. Ranyuk and P.V. Sorokin, J. Nucl. Phys. (USSR) **5**, 37 (1967) [Sov. J. Nucl. Phys. **5**, 26 (1967)].

[36] A.V. Mitrofanova, Yu. N. Ranyuk, and P.V. Sorokin, Yad. Fiz. **6**, 703 (1967) [Sov. J. Nucl. Phys. **6**, 512 (1968)].

[37] J.B. Martins, E.L. Moreira, O.A.P. Tavares, J.L. Vieira, L. Casano, A. D'Angelo, C. Schaerf, M.L. Terranova, D. Babusci, and B. Girolami, Phys. Rev. C **44**, 354 (1991).

[38] M.L. Terranova, O.A.P. Tavares, G.Ya. Kezerashvili, V.A. Kiselev, A.M. Milov, N.Yu. Muchnoi, A.I. Naumenkov, V.V. Petrov, I.A. Protopopov, E.A. Simonov, E. de Paiva, and E.L. Moreira, J. Phys. G: Nucl. Part. Phys. **22**, 511 (1996).

[39] M.L. Terranova, G.Ya. Kezerashivili, A.M. Milov, S.I. Mishnev, N.Yu. Muchnoi, A.I. Naumenkov, I.Ya. Protopopov, E.A. Simonov, D.N. Shatilov, O.A.P. Tavares, E. de Paiva, and E.L. Moreira, J. Phys. G: Nucl. Part. Phys. **24**, 205 (1998).

[40] W. Reisdorf, Z. Phys. A300 , 227 (1981).

Table 1: Comparison between calculated and experimental fissility values for ^{nat}Pb target nucleus at various incident photon energies.

Photon energy E_γ (GeV)	Average cascade residual[a] $\bar{Z}^*$ $\bar{A}^*$ $\bar{E}^*$(MeV)	Average first--chance fission probability[b] $\bar{f}_1(\%)$	Average experimental fissility[c] $\bar{f}_e(\%)$	Parameter $\bar{s}$[d]	Calculated fissility[e] $\bar{f}_c(\%)$	Relative deviation(%) $(\bar{f}_c - \bar{f}_e)/\bar{f}_e$
0.21	81 205 128	0.52±0.02	3.1±0.5	1.29±0.04	3.0±0.6	-3.2
0.26	81 204 153	0.71±0.08	3.5±0.4	1.30±0.06	3.9±1.1	11.4
0.28	81 204 163	0.80±0.08	4.4±0.4	1.31±0.03	4.2±0.7	-4.5
0.44	80 202 243	1.30±0.09	6.7±0.5	1.33±0.04	6.3±1.1	-6.0
0.47	80 202 258	1.42±0.08	6.4±0.5	1.33±0.03	6.9±0.9	7.8
0.49	80 202 268	1.42±0.07	6.4±0.5	1.33±0.03	6.9±0.9	7.8
0.54	80 201 293	1.26±0.07	6.8±0.4	1.33±0.03	6.1±0.8	-10.3
0.58	80 201 313	1.35±0.08	7.3±0.3	1.33±0.03	6.5±0.8	-11.0
0.76	79 199 403	1.63±0.05	7.7±0.5	1.31±0.03	8.5±1.1	10.4
0.84	79 198 443	1.46±0.09	7.7±0.4	1.31±0.03	7.7±1.1	0
1.02	78 196 533	1.34±0.09	7.5±0.5*	1.29±0.02	7.7±0.9	2.7
1.22	77 194 633	1.12±0.08	7.8±0.3	1.27±0.02	7.1±0.9	-9.0
1.53	76 191 788	0.90±0.01	7.4±0.4	1.24±0.02	6.8±0.9	-8.1
1.67	75 189 840	1.00±0.02	7.5±0.4	1.23±0.02	8.1±1.2	8.0
1.78	75 188 840	0.81±0.02	7.3±0.6*	1.22±0.02	7.1±1.1	-2.7
1.97	74 186 840	0.77±0.03	7.1±0.5	1.21±0.01	7.3±0.7	2.8
2.04	74 185 840	0.70±0.01	7.1±0.4*	1.20±0.01	7.3±0.7	2.8
2.54	72 180 840	0.56±0.01	6.7±1.0*	1.18±0.01	7.2±0.9	7.5
2.70	71 178 840	0.49±0.02	6.8±0.8	1.17±0.01	7.1±1.0	4.4
2.80	71 177 840	0.50±0.02	7.2±1.0*	1.17±0.01	7.3±1.0	1.4
3.01	70 175 840	0.464±0.001	7.1±1.0	1.16±0.01	7.8±1.2	9.8
3.05	70 174 840	0.48±0.01	7.3±1.2*	1.16±0.01	8.1±1.3	11.0
3.56	68 169 840	0.366±0.004	7.8±1.3*	1.15±0.01	7.3±1.4	-6.4
3.78	67 167 840	0.38±0.01	7.5±0.9	1.15±0.01	7.6±1.4	1.3
4.50	64 159 840	0.37±0.01	-	1.14±0.01†	8.2±1.2	-
5.00	62 153 840	0.36±0.01	-	1.14±0.01†	8.4±1.3	-
5.50	60 148 840	0.28±0.01	-	1.13±0.01†	8.1±1.3	-
6.04	58 142 840	0.28±0.01	-	1.13±0.01†	7.0±1.2	-

Table 1(continued)

———————————————

[a]Values obtained by using Eqs. (6-8). For ^{nat}Pb, E_c^n=44.6MeV, E_c^p=50.4MeV, and B=1629MeV.

[b]Calculated by Eq. (29).

[c]These are mean values between relative and absolute ^{nat}Pb fissility (full and open circles, respectively, in Fig. 6).

*Interpolated values.

[c]Values taken from the full line in the inset within Fig. 6.

†Extrapolated values.

[e]Calculated by Eq. (28).

Table 2: Comparison between calculated and experimental fissility values for ^{232}Th target nucleus at various incident photon energies.

Photon energy	Average cascade residual[a]			Average first--chance fission probability[b]	Experimental fissility[c]	Parameter	Calculated fissility[e]	Relative deviation(%)
E_γ (GeV)	$\bar{Z}^*$	$\bar{A}^*$	$\bar{E}^*$(MeV)	$\bar{f}_1$	$\bar{f}_e$	$\bar{s}$[d]	$\bar{f}_c$	$(\bar{f}_c - \bar{f}_e)/\bar{f}_e$
0.20	89	230	124	0.246±0.029	0.47±0.04*	1.77±0.16	0.50±0.10	6.4
0.21	89	230	128	0.239±0.025	0.48 ±0.03	1.83±0.12	0.46±0.07	-4.2
0.25	89	229	150	0.334±0.015	0.50±0.02*	2.07±0.12	0.54±0.05	8.0
0.26	89	229	153	0.330±0.014	0.56 ±0.03	2.09±0.10	0.52±0.04	-7.1
0.28	89	229	165	0.322±0.012	0.49±0.02	2.12±0.11	0.50±0.04	2.0
0.31	89	229	180	0.312±0.011	0.52±002	2.08±0.08	0.50±0.03	-3.8
0.54	88	226	296	0.251±0.017	0.53±0.01	1.74±0.06	0.53±0.05	0
0.76	87	224	407	0.174±0.011	0.50±0.01	1.55±0.04	0.48±0.04	-4.0
0.84	87	223	443	0.173±0.004	0.48±0.01	1.51±0.02	0.51±0.02	6.3
1.04	86	221	540	0.103±0.004	0.47±0.01*	1.36±0.01	0.45±0.02	-4.2
1.31	85	218	680	$(6.59\pm0.10)10^{-2}$	0.46±0.01*	1.252±0.004	0.46±0.01	0
1.59	84	215	820	$(4.83\pm0.19)10^{-2}$	0.45±0.01*	1.220±0.005	0.42±0.02	-6.7
1.79	83	213	907	$(4.96\pm0.31)10^{-2}$	0.44±0.01*	1.220±0.008	0.43±0.04	-2.3
2.14	82	209	907	$(3.91\pm0.09)10^{-2}$	0.41±0.01	1.199±0.003	0.41±0.02	0
2.42	81	206	907	$(3.41\pm0.10)10^{-2}$	0.38±0.02	1.190±0.006	0.39±0.03	2.6
2.63	80	204	907	$(2.79\pm0.04)10^{-2}$	0.38±0.02*	1.174±0.004	0.38±0.02	0
2.84	79	202	907	$(2.17\pm0.02)10^{-2}$	0.38±0.02*	1.157±0.003	0.38±0.02	0
3.10	78	199	907	$(1.51\pm0.04)10^{-2}$	0.39±0.02*	1.138±0.002	0.39±0.02	0
3.46	77	195	907	$(1.30\pm0.04)10^{-2}$	0.40±0.02	1.132±0.002	0.40±0.03	0
3.74	76	192	907	$(1.19\pm0.02)10^{-2}$	0.40±0.02*	1.129±0.002	0.40±0.03	0
4.22	74	187	907	$(7.85\pm0.21)10^{-3}$	-	1.118±0.001[†]	0.41±0.02	-
4.68	72	182	907	$(6.28\pm0.04)10^{-3}$	-	1.115±0.001[†]	0.39±0.02	-
5.05	71	178	907	$(5.43\pm0.14)10^{-3}$	-	1.112±0.001[†]	0.41±0.03	-

Table 2 (continued)

---

[a]Values obtained by using Eqs. (6-8). For ^{232}Th, E_c^n=44.6 MeV, E_c^p=51.0, and B=1767 MeV.

[b]Calculated by Eq. (29).

[c]These are values represented as full circles in Fig. 7.

*Interpolated values.

[d]Values taken from the full line in the inset within Fig. 7.

†Extrapolated values.

[e]Calculated by Eq. (28).

Figure captions

Fig.1 - Average excitation energy, $\bar{E}^*$(a), number of cascade protons, $\bar{N}_p^c$ (b), and neutrons, $\bar{N}_n^c$(c) produced in $^{\rm nat}$Pb $\equiv^{207}$Pb target plotted against incident photon energy, E_γ (upper scale). Part d (lower scale) shows the position of the average cascade residuals in a $Z \times N$ graph as compared with nuclides of the beta-stability line. Note an average excess of 2 neutrons in the produced residuals.

Fig.2 - Schematic representation of the evaporation-fission competition process from an excited, cascade residual ($\bar{Z}^*, \bar{A}^*, \bar{E}^*$). The meaning of the symbols is explained in the text (section 2.2).

Fig.3 - Chance-fission probability, q_{ni}, plotted against the order of generation of evaporation residuals, n, for 1.02-GeV incident photon on $^{\rm nat}$Pb. The extreme evaporation paths are indicated by the full straight lines of slopes s_m and s_l, and the evaporation path on which the equivalent, average residuals of each generation are located is represented by the dashed line of slope $\bar{s}$. Points represent calculated q_{ni}-values following the routine described in sections 2.3–2.5.

Fig.4 - The same as in Fig. 3 for different incident photon energies.

Fig.5 - The same as in Fig. 3 for a number of photoreactions in ^{232}Th target.

Fig.6 - Fissility of $^{\rm nat}$Pb versus photon energy. Full circles represent the fissility-values relative to those of ^{237}Np (i.e., $f_{\rm Np} \approx 1$) measured by Cetina *et al.* [10]; open circles are the absolute fissility-values obtained from the total photoabsorption cross section for $^{\rm nat}$Pb as explained in the text. The full line is the smooth, semiempirical fissility-curve as obtained in the present work in the range $\sim$0.2−3.8 GeV, and the dash-dotted line is the prediction up to 6 GeV (the shaded area indicates the associated uncertainty). The dotted line is the result using the RELDIS code (variant B) as reported in [16]. Experimental fissility data at lower energies are taken from [35,36] (squares), [37] (triangle), and [38,39] (diamonds), and the dashed line is a trend drawn by eye through these points. In the inset, points represent the semiempirical $\bar{s}$-values obtained from the average experimental fissilities ($\bar{f}_e$-values); the full line is a least-squares fit to these points, and the dotted line is the trend of $\bar{s}$ when only the relative fissilities are considered.

Fig.7 - The same as in Fig. 6 for ^{232}Th. Full circles represent the fissility-values (relative to ^{237}Np) measured by Cetina *et al.*[10]; open circles are the experimental data from

68 to 264 MeV measured at SAL by Sanabria *et al.*[15]. The full line represents the smooth, calculated fissility-curve in the range ∼0.2−3.8 GeV using the approach of the present work. The dash-dotted line is the prediction up to 5 GeV (the shaded area shows the associated uncertainty). The dotted line is the result using the RELDIS code (variant B) as reported in [16]. In the inset, the semiempirical $\bar{s}$-values are represented as full circles with error bars, and the full line is a smooth trend through these points.

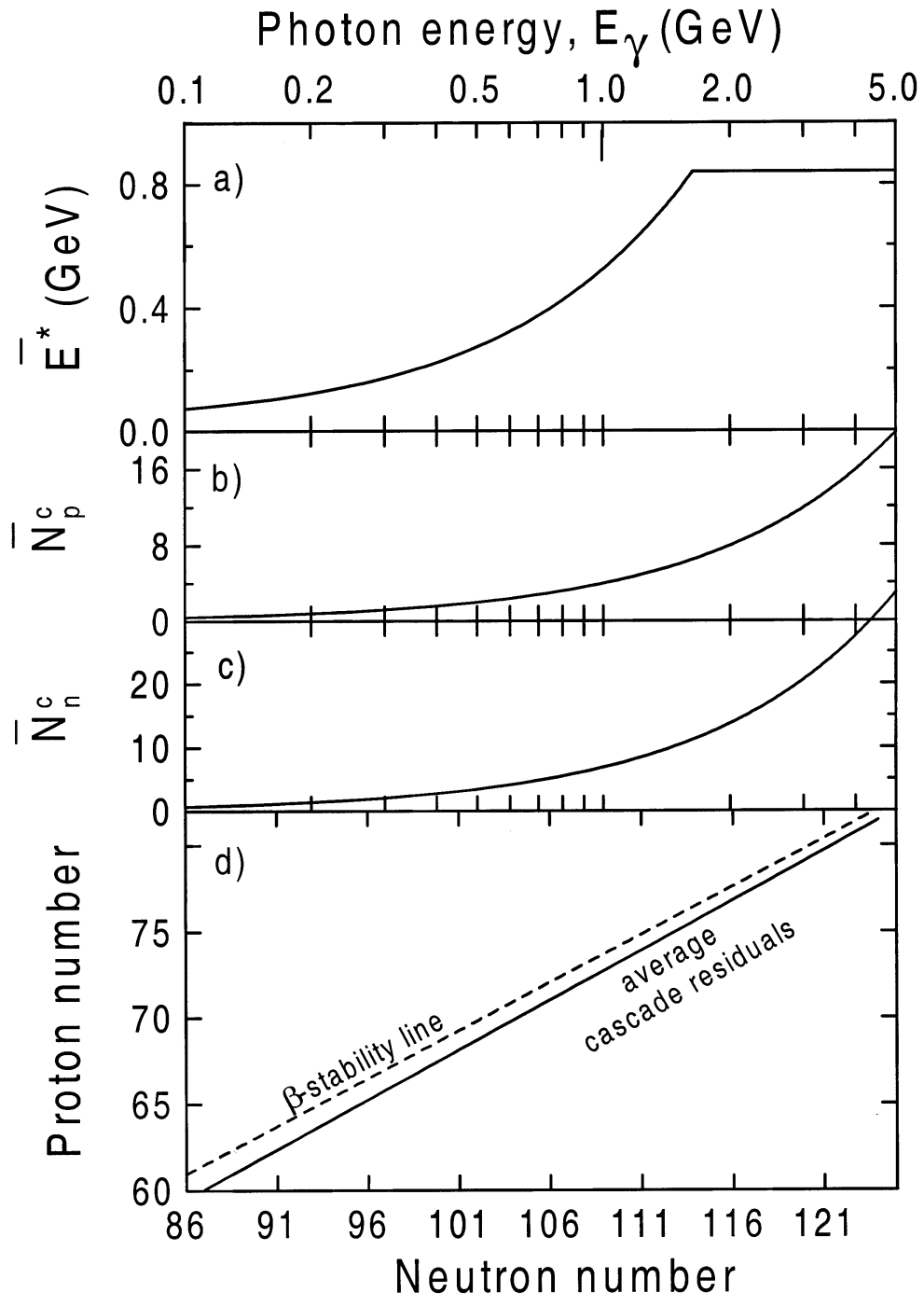
Photon energy, E_γ (GeV)
0.1
0.2
0.5
1.0
2.0
5.0
a)
$\bar{E}^*$ (GeV)
0.8
0.4
0.0
b)
$\bar{N}_p^c$
16
8
0
c)
$\bar{N}_n^c$
20
10
0
d)
Proton number
75
70
65
60
β-stability line
average
cascade residuals
86
91
96
101
106
111
116
121
Neutron number

Fig. 1

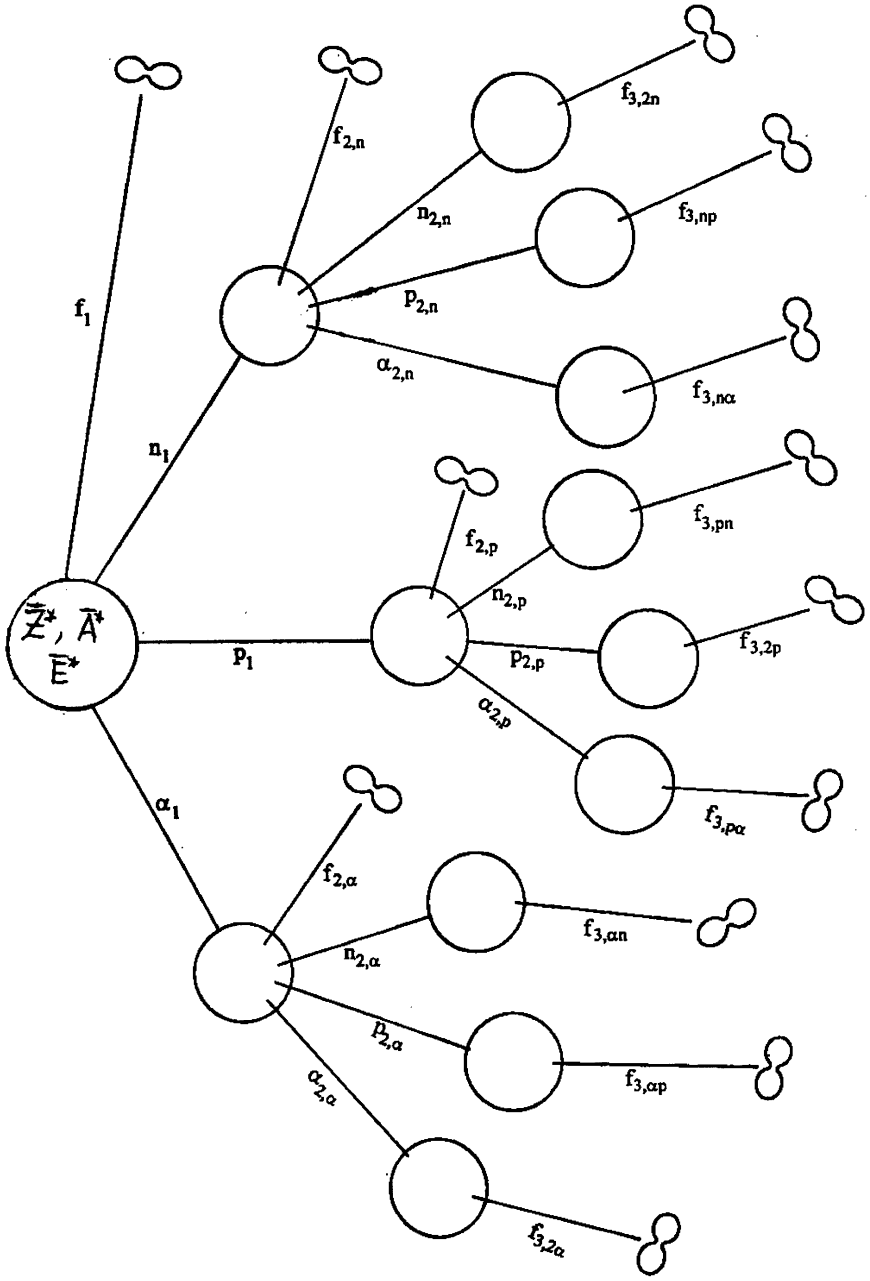
f1
n1
p1
α1
f2,n
n2,n
p2,n
α2,n
f3,2n
f3,np
f3,nα
f2,p
n2,p
p2,p
α2,p
f3,pn
f3,2p
f3,pα
f2,α
n2,α
p2,α
α2,α
f3,αn
f3,αp
f3,2α

Fig. 2

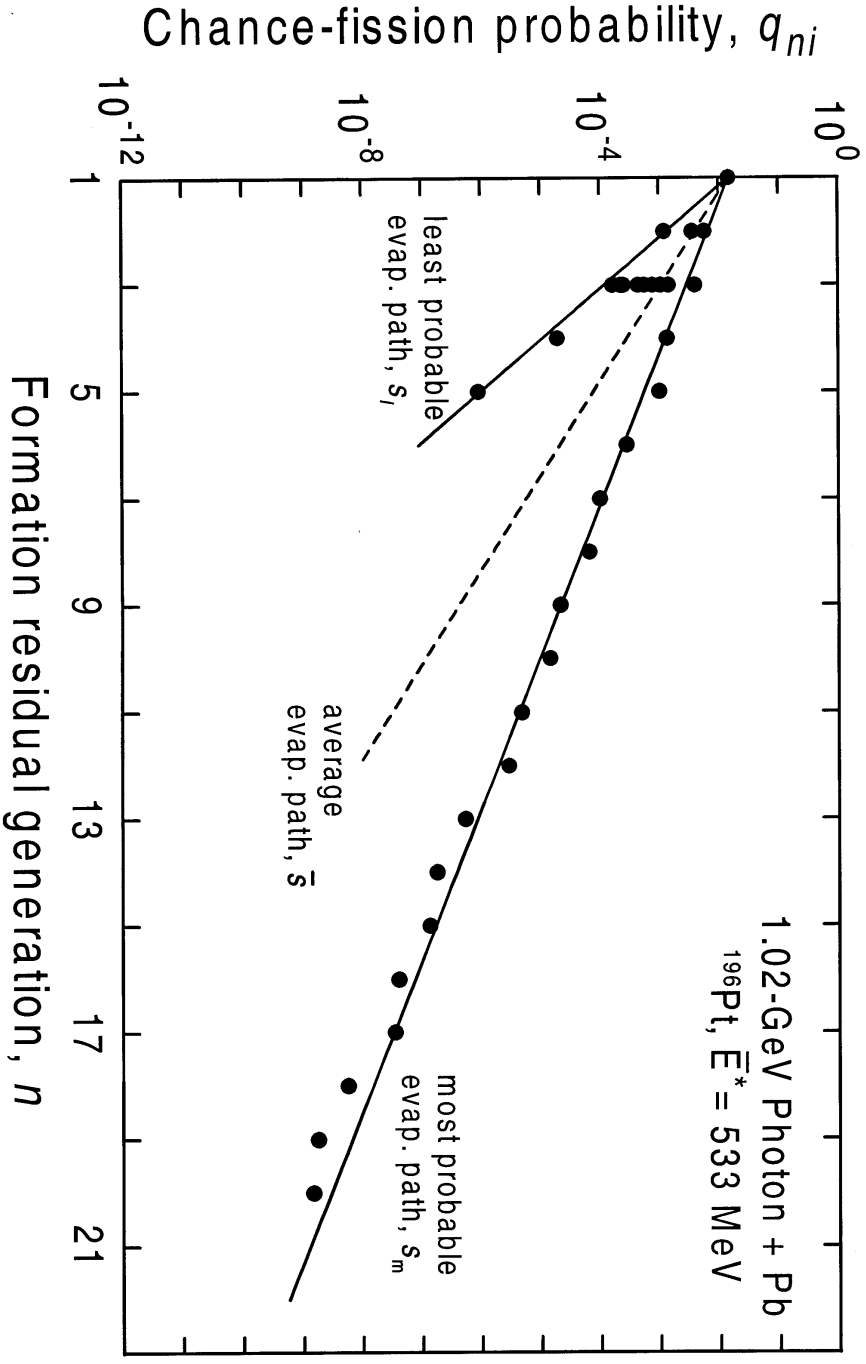
Chance-fission probability, q_{ni}
10^{0}
10^{-4}
10^{-8}
10^{-12}
1
5
9
13
17
21
Formation residual generation, n
1.02-GeV Photon + Pb
^{196}Pt, $\bar{E}^{*}$ = 533 MeV
least probable
evap. path, s_l
average
evap. path, $\bar{s}$
most probable
evap. path, s_m

Fig. 3

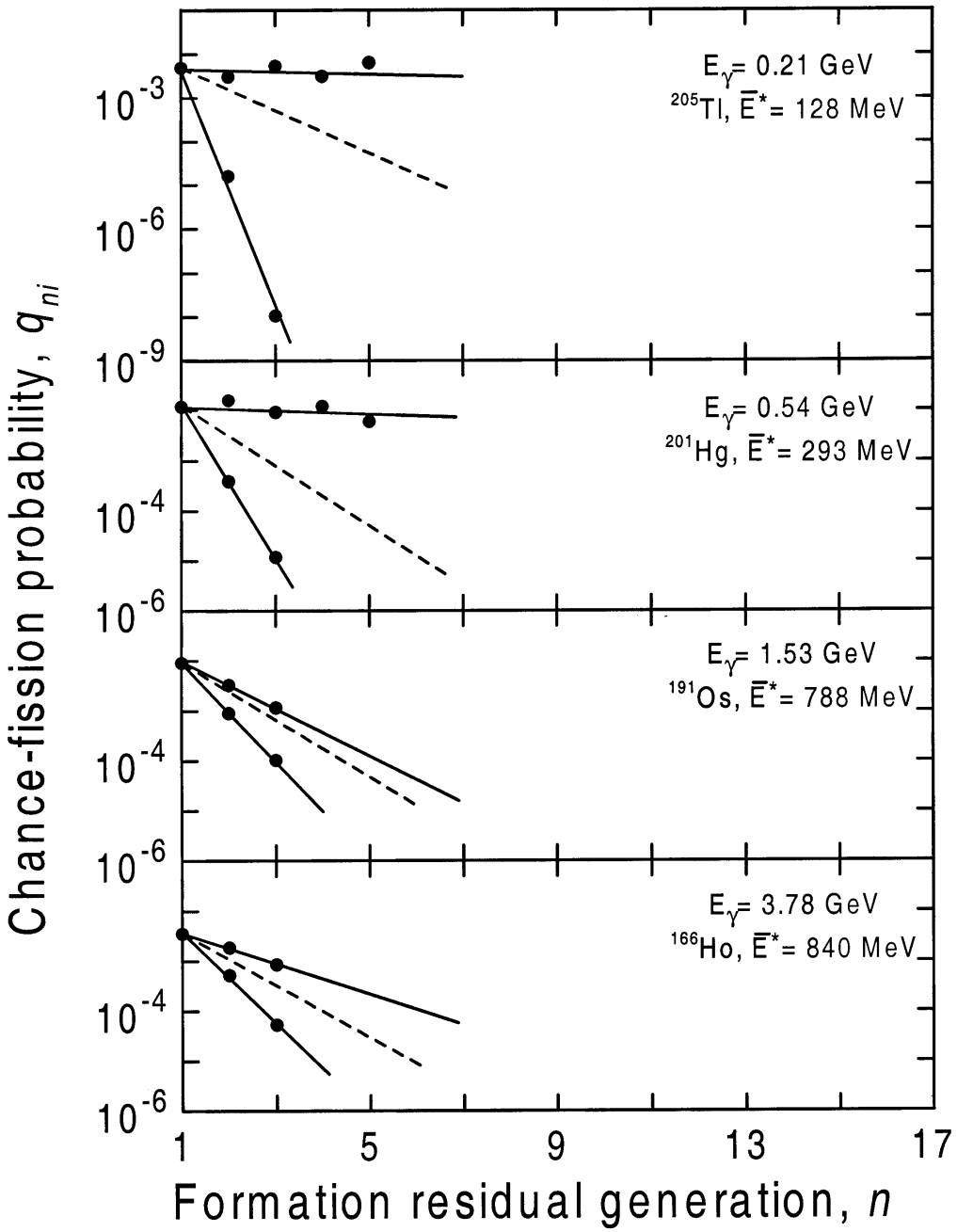
Chance-fission probability, q_{ni}
E_γ= 0.21 GeV
^{205}Tl, $\bar{E}^*$= 128 MeV
E_γ= 0.54 GeV
^{201}Hg, $\bar{E}^*$= 293 MeV
E_γ= 1.53 GeV
^{191}Os, $\bar{E}^*$= 788 MeV
E_γ= 3.78 GeV
^{166}Ho, $\bar{E}^*$= 840 MeV
10^{-3}
10^{-6}
10^{-9}
10^{-4}
10^{-6}
10^{-4}
10^{-6}
10^{-4}
10^{-6}
1
5
9
13
17
Formation residual generation, n

Fig. 4

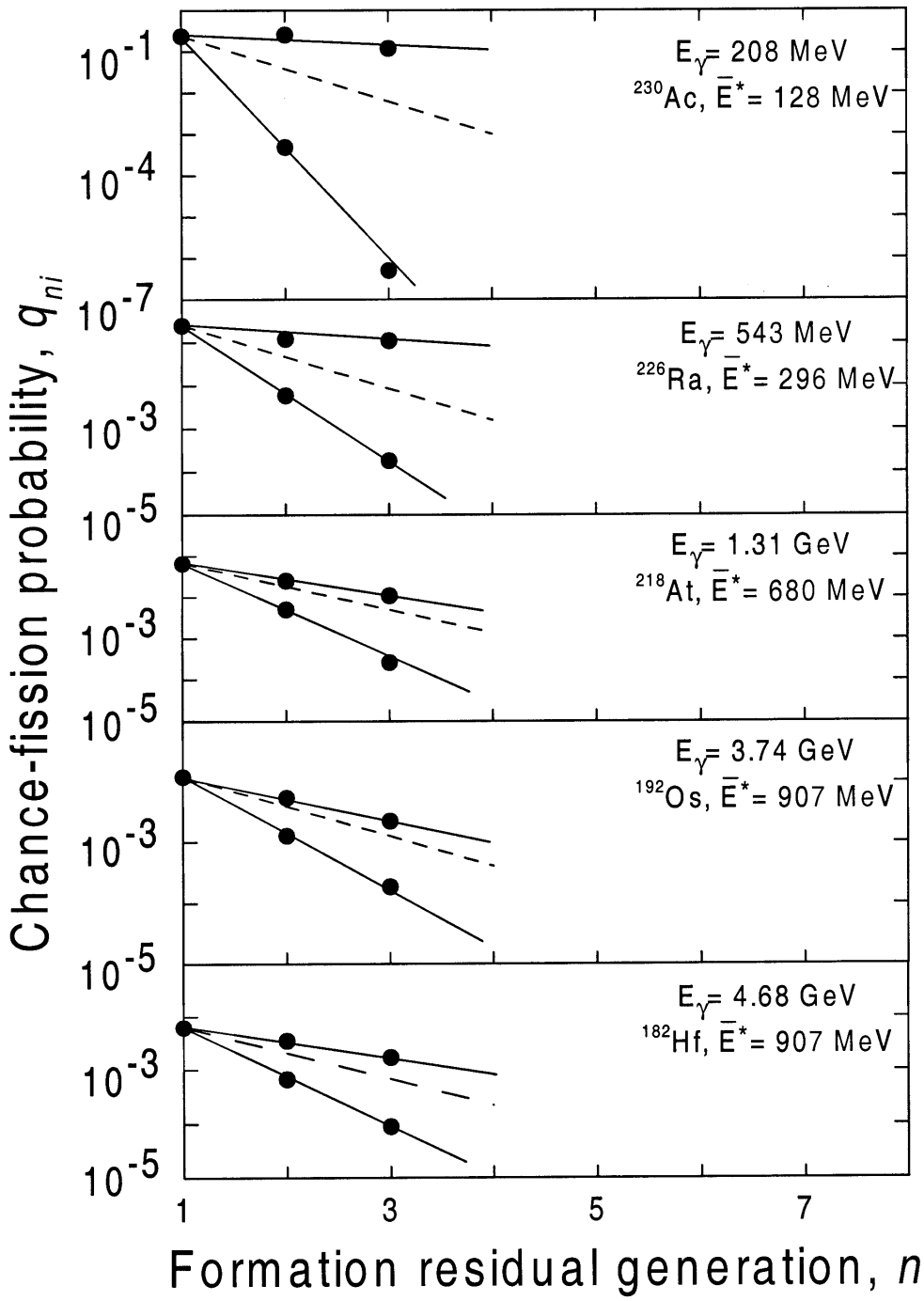
Chance-fission probability, q_{ni}
10^{-1}
10^{-4}
10^{-7}
10^{-3}
10^{-5}
10^{-3}
10^{-5}
10^{-3}
10^{-5}
10^{-3}
10^{-5}
E_γ= 208 MeV
^{230}Ac, $\bar{E}^*$= 128 MeV
E_γ= 543 MeV
^{226}Ra, $\bar{E}^*$= 296 MeV
E_γ= 1.31 GeV
^{218}At, $\bar{E}^*$= 680 MeV
E_γ= 3.74 GeV
^{192}Os, $\bar{E}^*$= 907 MeV
E_γ= 4.68 GeV
^{182}Hf, $\bar{E}^*$= 907 MeV
1
3
5
7
Formation residual generation, n

Fig. 5

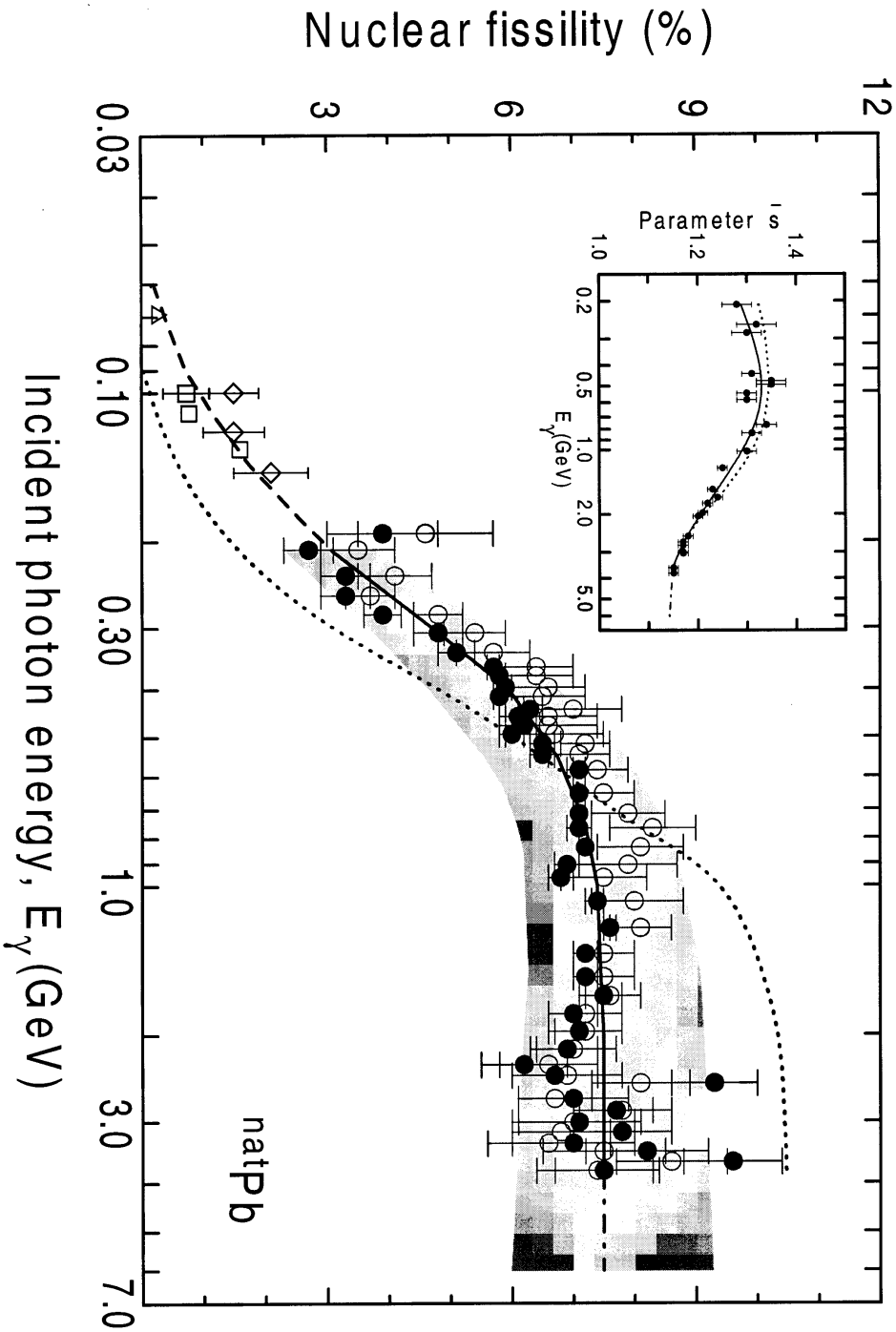
Nuclear fissility (%)
3
6
9
12
0.03
0.10
0.30
1.0
3.0
7.0
Incident photon energy, E_γ(GeV)
natPb
Parameter s
1.0
1.2
1.4
0.2
0.5
1.0
2.0
5.0
E_γ(GeV)

Fig. 6

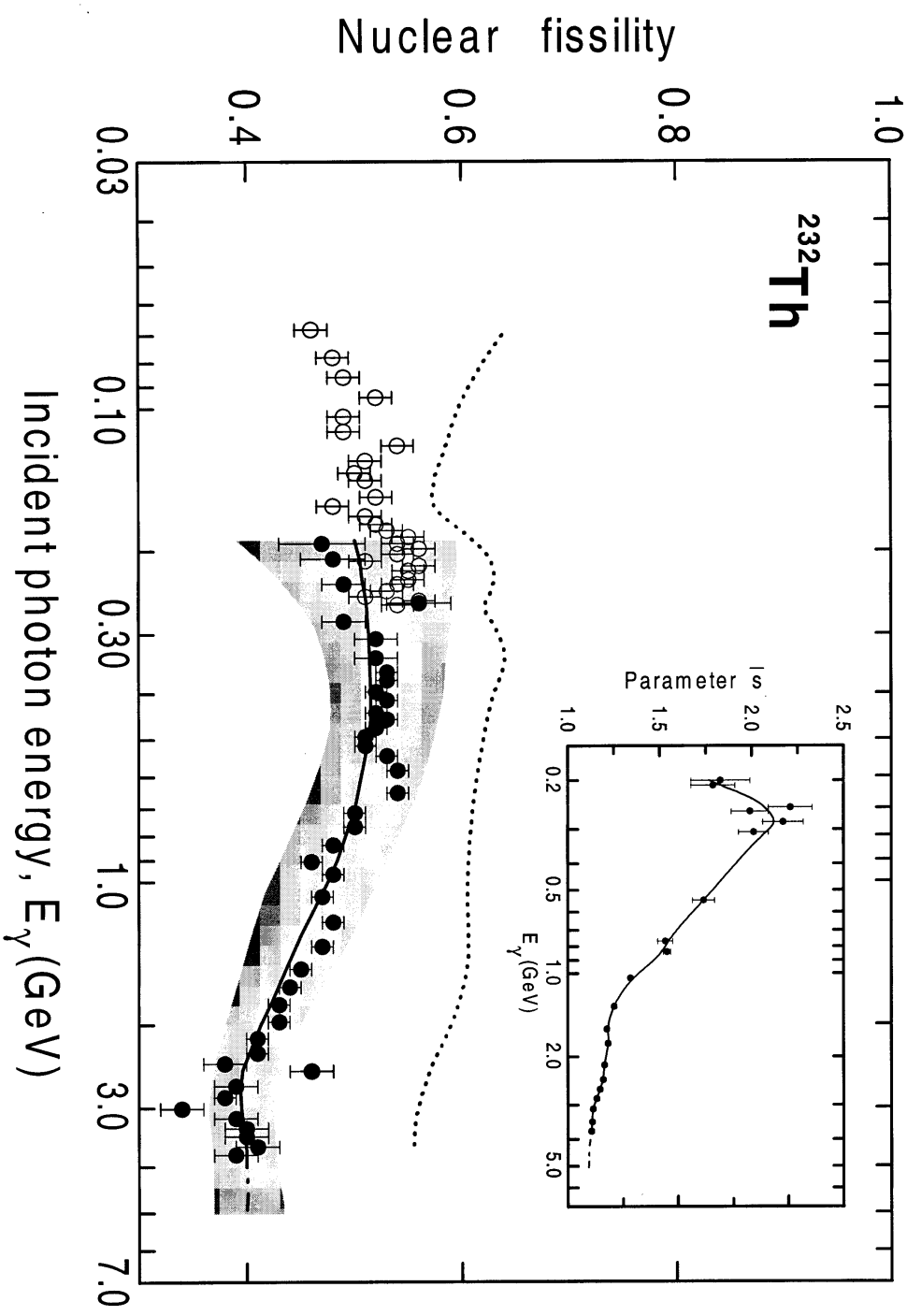
Nuclear fissility
0.4
0.6
0.8
1.0
0.03
0.10
0.30
1.0
3.0
7.0
Incident photon energy, E_γ(GeV)
^{232}Th
Parameter s
1.0
1.5
2.0
2.5
0.2
0.5
1.0
2.0
5.0
E_γ(GeV)

Fig. 7